

METHODS AND APPLICATIONS

Assembly of anthrax toxin pore: Lethal-factor complexes into lipid nanodiscs

N. Akkaladevi,¹ L. Hinton-Chollet,¹ H. Katayama,¹ J. Mitchell,¹ L. Szerszen,²
S. Mukherjee,¹ E. P. Gogol,² B. L. Pentelute,³ R. J. Collier,³ and M. T. Fisher^{1*}

¹Department of Biochemistry, University of Kansas Medical Center, Kansas City, Kansas

²School of Biological Sciences, University of Missouri Kansas City, Kansas City, Missouri

³Department of Microbiology and Immunobiology, Harvard Medical School, Boston, Massachusetts

Received 4 October 2012; Accepted 28 January 2013

DOI: 10.1002/pro.2231

Published online 7 February 2013 proteinscience.org

Abstract: We have devised a procedure to incorporate the anthrax protective antigen (PA) pore complexed with the N-terminal domain of anthrax lethal factor (LF_N) into lipid nanodiscs and analyzed the resulting complexes by negative-stain electron microscopy. Insertion into nanodiscs was performed without relying on primary and secondary detergent screens. The preparations were relatively pure, and the percentage of PA pore inserted into nanodiscs on EM grids was high (~43%). Three-dimensional analysis of negatively stained single particles revealed the LF_N-PA nanodisc complex mirroring the previous unliganded PA pore nanodisc structure, but with additional protein density consistent with multiple bound LF_N molecules on the PA cap region. The assembly procedure will facilitate collection of higher resolution cryo-EM LF_N-PA nanodisc structures and use of advanced automated particle selection methods.

Keywords: lipid nanodiscs; lethal factor; protective antigen; electron microscopy

Introduction

Bacillus anthracis synthesizes three monomeric proteins that combine to create a formidable protein toxin, anthrax toxin. One of the proteins, called the protective antigen (PA, 83 kDa), binds to either of two cellular receptors and is then cleaved by a cellular

protease to form a 63 kDa monomeric form, which oligomerizes to form heptamers and octamers on the cell surface. The other two proteins, lethal factor (LF) and edema factor (EF), are enzymes that act on cytosolic substrates. LF and EF bind competitively to oligomeric PA with a stoichiometry of 1 mol LF or EF per 2 PA monomers. At high concentrations these factors drive PA dimer formation and shift the assembly pathway to favor formation of octameric, as opposed to heptameric, structures on the cell surface.^{1,2} Heptameric or octameric PA with the bound LF and or EF cargo is endocytosed, and upon acidification, the PA oligomer transitions from a soluble prepore to a translocation-competent, membrane-inserted pore. The pH

Additional Supporting Information may be found in the online version of this article.

Grant sponsor: NIH; Grant number: R56 R56AI090085, R01AI090085, SR37AI022021.

*Correspondence to: M. T. Fisher, Department of Biochemistry, University of Kansas Medical Center, Kansas City, KS. E-mail: mfisher1@kumc.edu

gradient between the endosome lumen and the cytoplasm drives the unfolding and translocation of the ~90 kDa lethal and edema factors³ across the endosomal membrane. Once translocated, the factors refold, perhaps with the assistance of cytoplasmic chaperones, and modify their respective substrates, disrupting key cellular processes.⁴

In order to understand this fundamentally important translocation process, it is necessary to determine the molecular structure of the PA translocon and its bound cargo proteins. Ultimately, our goal is to obtain three-dimensional structures at a resolution sufficient to map the physio-chemical landscape of the lumen of the translocon. This map will allow us to employ techniques, such as steered molecular dynamics, and derive energy potential functions to understand how this exquisite electrostatic machine accomplishes rapid pH-driven unfolding and directional translocation of the enzymic anthrax effector proteins. Thus far, mapping the lumen has depended upon low resolution structures of the membrane-insertable forms of the PA pore obtained by single-particle reconstruction electron microscopy techniques.^{5,6} In one study, we used the limits imposed by the electron density obtained from EM to apply structure targeted normal mode flexible fitting (NMFF) approaches⁶ to localize interior protein densities that appear to correspond to the critical phenylalanine clamp region.¹ This latter region plays a key role in gating translocation and may chaperone the unfolded protein through this constriction region. Recent data from electron paramagnetic resonance studies and from chemical crosslinking provide biochemical evidence that the unstructured N-terminal portion of the lethal factor resides at or near this constricted clamp region prior to translocation.⁷

Given the inherent difficulties in crystallizing the functional pore, an alternative approach is to obtain moderate-to-high resolution cryoEM derived structures. For instance, the structure of the highly symmetric tetradecameric protein GroEL has been solved using cryoEM methods at a resolution of 4 Å. GroEL is a dimer of symmetrical heptameric rings, allowing one to use minimally tilted populations of side views while still covering all rotational space for single particle reconstructions.⁸ Similarly, it was found that the PA pore-heptamer-nanodisc structure fortuitously orientates on the carbon-coated EM grid in side view orientations. This allows one to use approaches similar to those used with GroEL to collect population images at shallow tilt angles and apply symmetry operations to reconstruct the PA pore nanodisc structures. Previous work along these lines yielded a low-resolution PA-nanodisc structure using negative stain EM single particle structure analysis.⁶ However, the original PA nanodisc sample was highly heterogeneous, containing PA pore

inserted into nanodiscs, PA pore inserted into vesicles, aggregated PA pores and prepores, empty vesicles, and free nanodiscs. A superior method was therefore needed to acquire more highly enriched PA-nanodisc samples for cryoEM analysis.

To this end, we devised a method for inserting the anthrax toxin PA pore into lipid nanodiscs that avoids laborious detergent screens, prevents large-scale aggregation, and yields relatively pure LF_N-PA pore nanodisc complexes. First we covalently linked a mutated, single-Cys form of LF_N onto a cross-linked agarose surface via a disulfide bridge and allowed prepore to bind to the immobilized LF_N via sites on the prepore cap. The bound prepore was then induced to transition to the pore state. Finally a lipid nanodisc was allowed to form around the exposed hydrophobic tip of the PA pore. The assembled complex was removed from the immobilized surface by disulfide reduction and evaluated using negative stain EM. The resulting samples contained only nanodiscs and LF_N-PA pore nanodisc complexes.

Adsorption of these nanodiscs and complexes to the solid carbon EM substrate yielded a high fraction (>50%) in an edge-view orientation, favorable for the analysis. These samples were also subjected to preliminary screens using cryoEM methods. In this latter instance, the purified LF_N-PA pore nanodisc complexes also fortuitously orientated on carbon as side views, thus allowing us to proceed with automated particle picking to obtain higher resolution LF_N-PA pore nanodisc structures. Single-particle image analysis of the negatively stained samples in combination with 3D reconstruction yielded a structure at 26-Å resolution. Although the LF_N-PA-nanodisc structure is observed to be similar to the previously determined PA-nanodisc structure,⁶ there is clear evidence that the bound LF_N protein contributes extra density to both the PA cap region and within the lumen of the PA pore cap.

Results

Previously we developed a method to initiate the transition from prepore to pore directly on Ni-NTA beads and the assembled nanodiscs around exposed hydrophobic pore tips.⁶ This approach gave a moderate yield of pore inserted into lipid nanodiscs, but with a substantial population of empty nanodiscs, lipid vesicles, PA pores inserted into lipid vesicles, and aggregates of both the prepore and pore. Since immobilization of the PA prepore would be predicted to diminish pore aggregation, we designed an alternative prepore-to-pore transition protocol involving first binding prepore to immobilized LF_N. The prepore could be captured by the immobilized LF_N by virtue of the high binding affinity ($K_d \sim 1$ nM) and the prepore induced to transition to the pore state

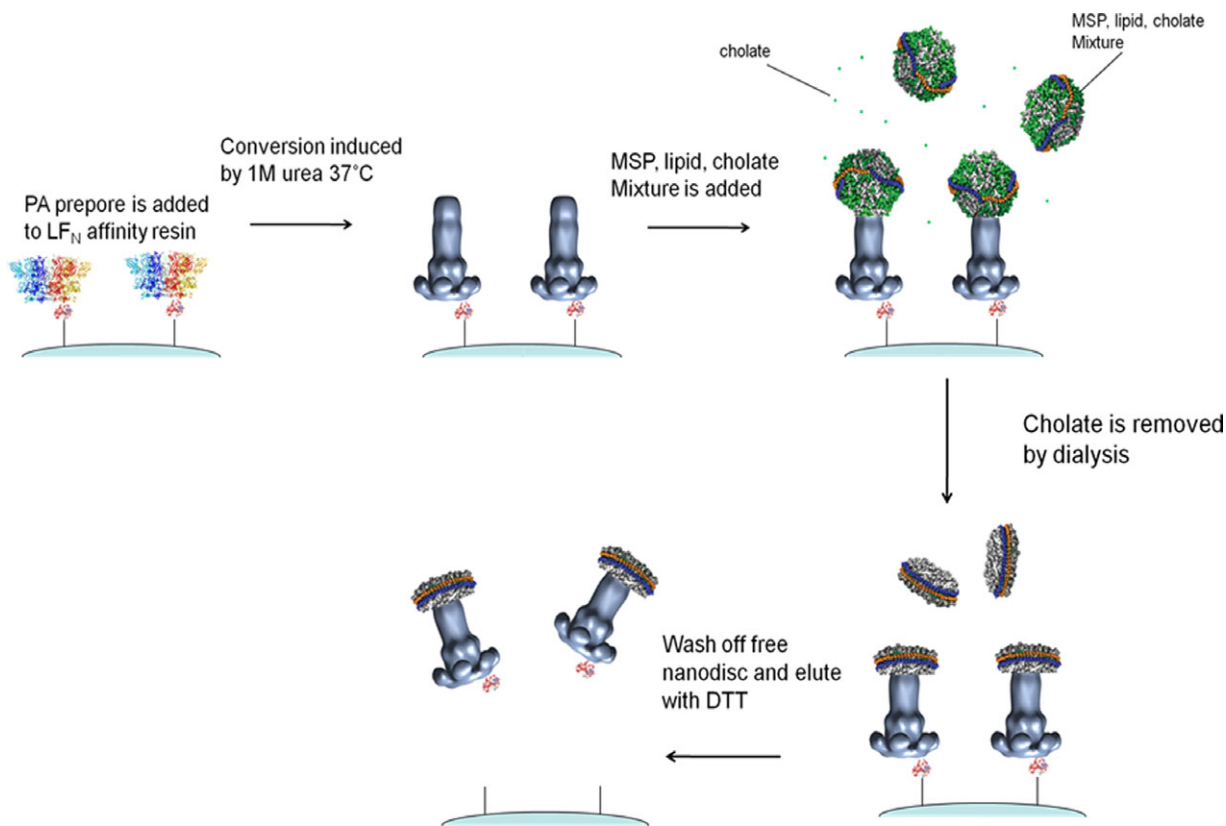


Figure 1. Affinity purification of LF_N-PA-nanodisc complex on immobilized solid support. PA prepore (1TZO) binds to LF_N (N terminal domain 1JZN) beads and stays bound during the washes and buffer exchange. Prepore to pore conversion is induced on same support and lipid nanodiscs are formed around the exposed hydrophobic tip. Finally LF_N-PA-nanodisc complex eluted with DTT.

while bound to LF_N. The pore's extended beta barrel structure was predicted to extend ~100 Å away from the support surface, reducing the potential for aggregation. After this conversion, nanodiscs could be formed around the exposed hydrophobic tip of the pore, which functions in membrane insertion (Fig. 1).

To identify a suitable affinity resin for the prepore, we first prepared two single-cysteine forms of LF_N (E126C, R263C) and reacted each with activated thiol-Sepharose 4B. Based on the fact that the lumen of the prepore (and the pore) is negatively charged and binds the unstructured cationic N-terminal regions of LF and EF, we also prepared a third candidate affinity resin generated by reacting a synthetic single-Cys peptide containing a polycationic tract at the N terminus (KKKKKAGNAGANAGAGC) with activated thiol-Sepharose.⁷ When these three candidate resins were tested, the E126C construct was found to have the highest binding efficiency for the prepore. Retention of PA on LF_N E126C beads was most efficient in buffer that contained 50 mM NaCl, pH 7.5. The prepore was not retained on polylysine beads, as reflected by poor PA nanodisc formation after overnight incubation.

The next steps involved converting the prepore to the pore and forming the nanodisc around the

exposed hydrophobic tip (Fig. 1). Prepore-to-pore conversion was induced by 1M urea at 37°C for 5 min on LF_N E126C affinity beads. Before and after conversion, the presence of PA from the supernatant of LF_N affinity beads was assessed by SDS-PAGE analysis. There was no protein in the supernatant after conversion from PA prepore to pore, suggesting that a significant amount of PA localized onto the bead surface (Supporting Information Fig. S1). The PA pore remained bound to lethal factor beads with its exposed hydrophobic tip projecting away from the support surface, preventing significant aggregation. If the PA pore was eluted from the beads by addition of DTT in the absence of lipids, aggregates were formed that resembled those of PA pore previously characterized [Supporting Information Fig. S2(A,B)]. After constructing the nanodiscs in the presence of the LF_N bead-immobilized PA pore, covalently attached complexes were eluted with DTT (see methods). To further eliminate any pores not bound to nanodiscs, a second affinity purification step on Ni-NTA affinity columns was performed, taking advantage of the MSP1D1 His tag. This second step selected for the His-tagged MSP, and the two-step affinity purification method yielded a sample with minimal pore aggregates and vesicles. Purified complex was assessed by negative stain electron

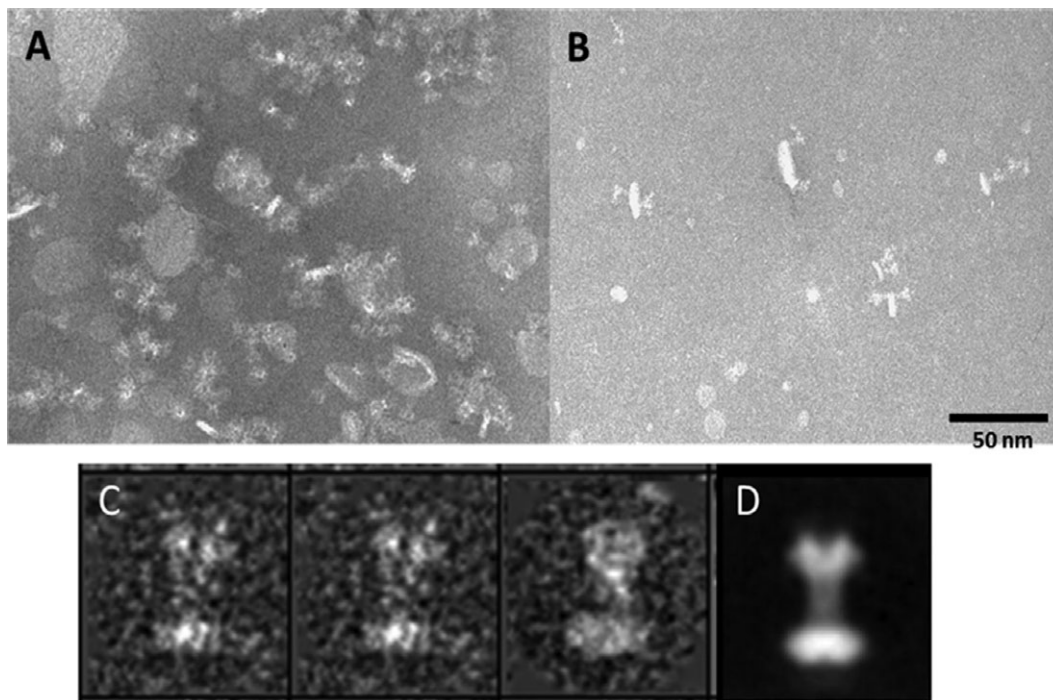


Figure 2. Comparative negative stain EM micrograph fields. (A) NTA-Ni immobilized PA nanodisc and contaminants. (B) Field of orientation generated LF_N-PA-nanodisc complexes (scale bar: 50 nm). Both fields were negatively stained with 1% methylamine tungstate and viewed at 60,000 \times using a JOEL 1200EX electron microscope. Note the loss of large aggregates and PA pore vesicle images. (C) Representative images depicting the orientation of the PA pore inserted lipid nanodisc. (D) Two-dimensional average of 901 LF_N-PA nanodiscs of eight population class images derived from *k*-means classification.

microscopy; comparative EM fields are shown in Figure 2. The apparent insertion yield of LF_N-PA complex into nanodisc was 40–50% as judged by visual inspection of several electron micrograph fields of independent preparations.

Initial analysis of the EM images was performed by manually selecting 1638 LF_N-PA-nanodisc complexes from 20 micrographs. All these particles were subjected to reference free 2D analysis and performed *k*-means classification using SPIDER,⁹ enabling separation into twenty classes, based primarily on differences in PA density and nanodisc size (Supporting Information Fig. S3). Eight of these classes, comprising 901 particles with PA density at a constant distance from the nanodisc, were used to generate the two-dimensional averages shown in Figure 2(B).

This small 901 image data set was used for a preliminary 3D analysis, yielding a structure [Fig. 3(A)] with a nominal resolution of 26 Å, estimated by Fourier shell correlation with a cutoff value of 0.5 (Supporting Information Fig. S4). The procedures used for particle selection and alignment, leading to three-dimensional reconstruction, have been described.⁶ The lower resolution of the EM reconstruction presented here is likely the result of the limited number of particles used. The structure is similar to that previously determined for unliganded PA pore inserted into nanodiscs⁶ as well that of the pore bound to GroEL⁵ namely a mushroom-shaped

protein complex extending away from the membrane. In the current reconstruction, the LF_N-PA complex is 190 Å long, including the nanodisc bilayer, and the seven-fold “cap” distal from the nanodisc is 140 Å in diameter. Both of these dimensions are approximately 10 Å larger than those of the previous unliganded reconstruction, presumably reflecting the LF_N bound to the cap of PA. The interior of the LF_N-PA cap structure appears to be filled with protein (i.e., stain exclusion) [Fig. 3(B)] compared to the unliganded PA in the previous publication.⁶ This difference is consistent with the insertion of the unstructured amino terminus of the LF_N into the translocon channel, as predicted by biochemical and biophysical studies.^{7,10}

The structure of the LF_N-PA complex was interpreted by fitting the PA pore NMFF structure⁶ into the EM densities. In contrast to our previous negative stain reconstruction of the unliganded PA-nanodisc complex, the region identified as PA domain 2 is not as well resolved, and PA domain 3 protrudes radially. It is not clear whether these differences are due to the lower nominal resolution of the latest reconstruction, or to conformational changes induced by LF binding. However, the resulting fit of the NMFF structural elements into the EM density yields a correlation coefficient of 0.8 (vs. 0.87) [Fig. 3(C)].⁶ Individual LF_N monomers are not resolved in this reconstruction, since it is anticipated that a

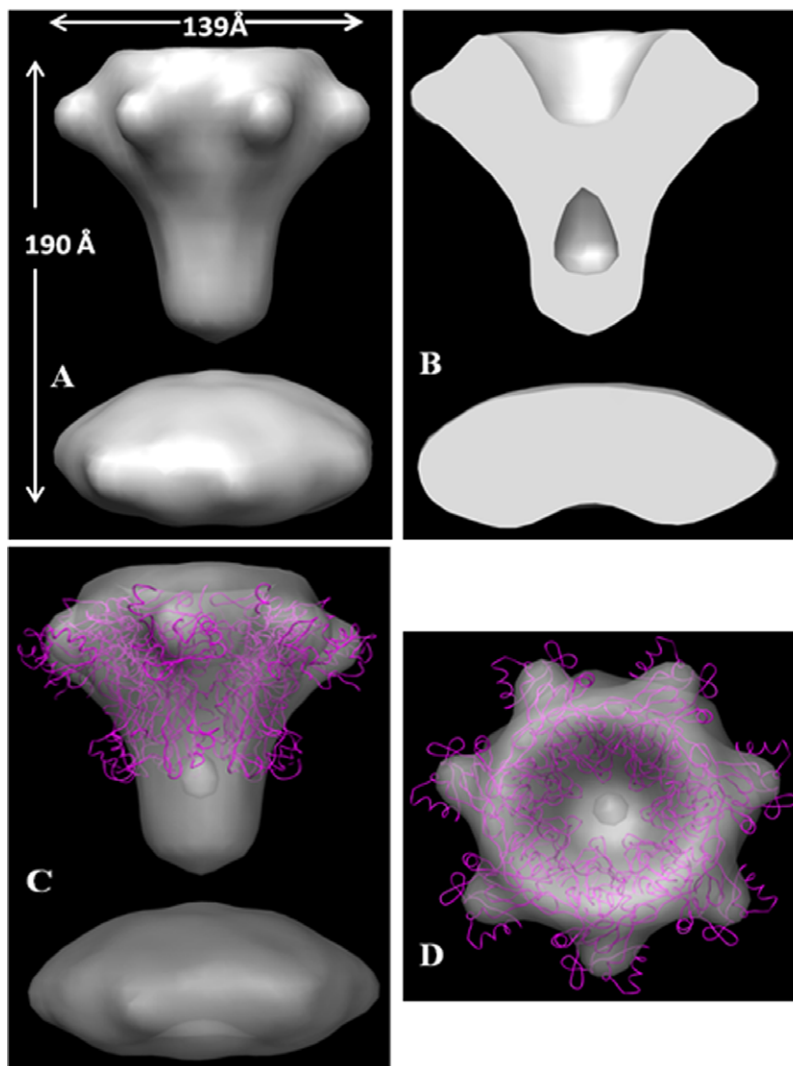


Figure 3. (A) Negative staining EM structure of the anthrax LF_N-PA at 26 Å. (B) Half slice view of the structure, with the red arrow indicating that extra density corresponding to LF_N near the Phe427 clamp region. Hand fit of PA pore (which is derived from crystal structure of PA prepared by NMFF analysis⁶) into LF_N-PA nanodisc EM density using Chimera; correlation coefficient is 0.8. (D) Top view and (E) side view.

total of three bound LF_N monomers would result in a smeared additional density because of the seven-fold symmetry operation imposed to calculate the structure.

To obtain higher resolution structures using electron microscopy, it is necessary to demonstrate that one can resolve individual images in representative cryosamples. As indicated by our negatively stained reconstructions, the side view orientations of the seven-fold symmetrized PA pore-nanodisc, and minimal tilts of that orientation, are adequate for a reasonable three-dimensional reconstruction of the pore.^{5,6} To assess the feasibility of using these specimens for cryo-EM analysis, we prepared unstained frozen specimens and collected initial sets of electron micrographs. Since very few edge-views of the nanodiscs (with or without PA inserted) were visible in cryoEM grids prepared with holey carbon films, we used holey films coated with a thin carbon layer,

yielding numerous edge-views [Fig. 4(A)]. Sample loading was improved by incubating the solutions on these grids for 1–2 min prior to blotting and freezing. Images collected either on film or on CCD camera exhibited nanodiscs of various sizes, and some of the raw images displayed projecting densities of the same overall shape and dimensions as the LF_N-PA reconstructions [Fig. 4(B)]. These preliminary observations indicate the feasibility of pursuing higher resolution cryoEM reconstruction of the nanodisc complexes.

Discussion

Membrane protein insertion into lipid nanodiscs is a powerful method for generating soluble complexes that can be purified by simple chromatographic methods. Detergent-solubilized proteins are often prone to denaturation by this standard reconstitution method. It is desirable to construct more

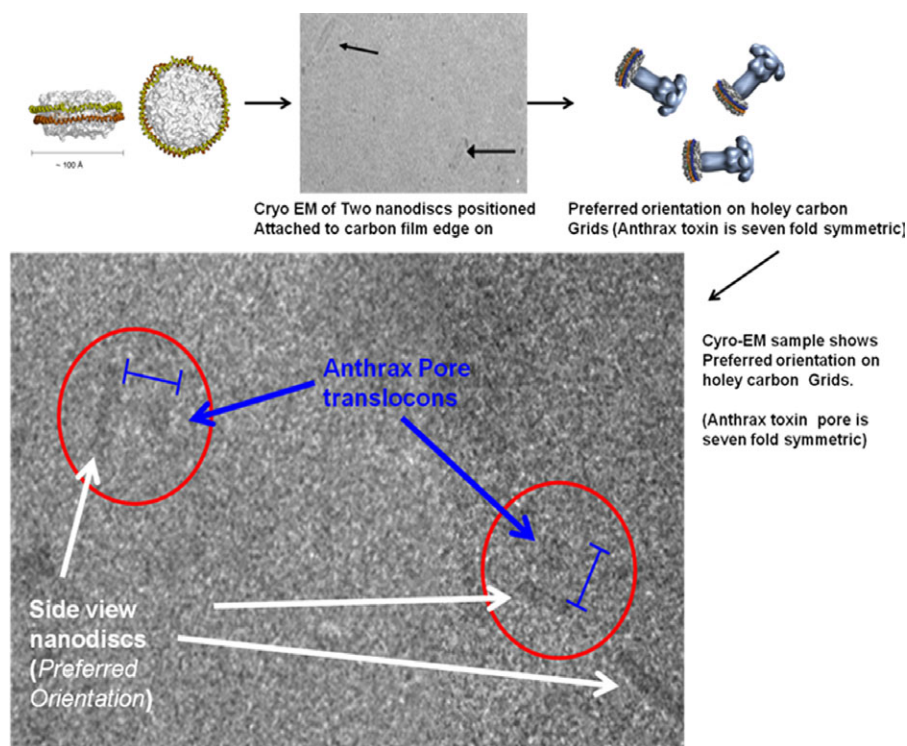


Figure 4. Nanodiscs and anthrax toxin translocon structures observed by cryo-EM. For the nanodiscs alone, the images were recorded on film (Kodak SO163) by using a minimal-dose protocol at a magnification of 60,000 \times with a JEOL 1200EX (UMKC – E. Gogol) electron microscope at a defocus of 0.6–0.7 μm . The cryo EM of PA pore images were recorded on Tecnai F20 electron microscope (FEI, Eindhoven, The Netherlands) operated at 200 kV and equipped with a Gatan cold stage (Gatan, USA) and recorded on a Gatan 1k CCD camera (Gatan, UK) at a magnification on the CCD camera of 60,000 \times with 0.6–0.5 μm underfocus. The cartoons are positioned to illustrate the preferred orientation with respect to the seven-fold symmetry axes of the PA pore inserted into the nanodisc (mushroom shaped protein from Ref. 5). The blue bars are 150 Å in length.

relevant physiological structures including lipid vesicles and lipid nanodiscs. The number of structures that use lipid nanodisc platforms is on the rise.^{11–15} Nanodisc-membrane protein structures have been assessed using NMR and more recently reasonable EM structures have been obtained, potentially yielding insights into membrane protein structures that have remained refractory to crystallographic efforts.^{6,16}

For EM in particular, it is anticipated that nanodiscs will provide benefits for eventually obtaining easily observed structures because nanodiscs, particularly in their side view orientations, are of high enough contrast to allow easier automated particle picking, ultimately leading to higher image numbers and hence resolution. As shown in Figure 4, the contrast of the nanodisc appears to be superior to the inserted PA pore although at this defocus value, the protein density of the PA pore can be barely observed. This enhanced contrast of the side view orientation of the nanodisc is due to the electron dense phospholipid head groups. One may be able to resolve a lower contrast image from the inserted protein if the inserted density is matched to a reference, and a translational search is made per-

pendicular to the nanodisc edge above and below the nanodisc. For negative staining, the contrast differences between the nanodisc and PA pore are not an issue.

Current protocols for assembling membrane protein-nanodisc complexes rely on the initial solubilization of the membrane protein to be inserted and simultaneous removal (usually by dialysis) of detergents from both the solubilized membrane protein and the detergent-lipid-matrix scaffold protein (MSP1D1) micelle. If all goes well, the membrane protein preferentially inserts into detergent-lipid-MSP complexes, avoiding large-scale off-pathway self aggregation. In current nanodisc membrane protein insertion protocols, an additional complicating issue that results in potential variability in the assembly steps results from detergent compatibility. The published protocol still carries a degree uncertainty for insertion success where the determining factor is highly dependent on detergent selection (i.e., screens) and the aggregation processes.¹⁷

Although the standard nanodisc preparation methods continue to yield highly pure and useful membrane protein lipid structures, we were unable

to garner success constructing PA-nanodisc complexes when using the known PA pore solubilizing detergent Fos14.¹⁸ Realizing that our previous successes in forming observable pores relied on constraining the prepore structure prior to pore transition,^{5,6} we surmised that generating a defined immobilized state of the PA prepore with its authentic truncated LF_N protein component should lead to adequate and relatively pure nanodisc PA complexes for EM structural analysis. Indeed, using this unique matrix-attached sulfhydryl linkage with the engineered LF_N E126C construct led to a vastly superior purification and insertion of the PA-nanodisc complex. The orientation of PA prepore enables one to transition, expose and extend the PA pore membrane insertion competent tip away from the bead surface into the solution phase. The nanodiscs assemble around the fully exposed PA hydrophobic membrane insertion tip. The most novel element of this procedure indicates that one can avoid extensive detergent screens and acquire large amounts of highly pure PA nanodiscs. In retrospect, the PA prepore is naturally immobilized by surface receptors prior to its transition to the pore state *in vivo*, insuring a proper directional insertion into the endosomal membrane. Thus, our *in vitro* immobilization method essentially recapitulates this directional transition, allowing us to avoid large scale aggregation and cumbersome detergent screens.

Although the EM structure of the LF_N-PA nanodisc complex is at low resolution (26 Å), it does point out features that are quite distinct from the previous negative stain structure of the PA pore nanodisc complex alone. The initial negative stain structure of the LF_N-PA nanodisc complex reveals the extra density contributed by LF_N binding. The interior cap region above the Phe427 clamp now contains an extensive stain-excluding area suggesting that the unstructured N-terminal tail of LF_N fills this upper cap region. As predicted, binding of the unstructured region of LF_N within the PA cap region appears to prevent stain from entering the internal lumen, but a portion of the remaining cavity is observed that appears to be positioned near the Phe427 flexible loop. On the cap ridge itself (where LF_N binds), there is additional density that cannot be attributed to NMFF estimates of the conformational readjustments of the PA pore cap⁶ (see Fig. 6 in Ref. ⁶). All other features of the PA pore nanodisc are essentially replicated starting from this purified sample.

It will be interesting to test the general applicability and success of our immobilization/nanodisc construction method with a broad range of membrane proteins. As a simple practical procedure, we predict that this immobilization procedure will be useful for other membrane protein-nanodisc constructions, provided one can specifically orient and immobilize membrane proteins on inert surfaces,

allowing one to fold and form nanodiscs around exposed membrane insertion regions. Employing immobilization/nanodisc construction procedures could be useful to assemble membrane-protein nanodisc complexes without employing tedious and time-consuming detergent screens. With the advent of numerous affinity immobilization tags, it is entirely conceivable that one could even refold oriented membrane proteins in the presence of the MSP/lipid/cholate micelle mixtures to generate large amounts of correctly inserted membrane protein-nanodisc complexes.

Methods

Materials

Expression and purification of proteins. Wild type PA was expressed recombinantly in the periplasm of *Escherichia coli* BL21 (DE3) and purified by anion exchange chromatography.¹⁹ PA prepore was purified by anion-exchange chromatography after activation of PA with trypsin.²⁰ QuikChange site-directed mutagenesis (stratagene) strategies was used to introduce mutation into plasmids [pET-SUMO (Invitrogen)] encoding recombinant LF_N E126C and LF_N R263C. These mutants were expressed as His6-SUMO-LF_N variants, which were later cleaved by SUMO (small ubiquitin-related modifier) protease, revealing the native LF_N E126C and LF_N R263C N terminus.⁷

Preparation affinity beads. LF_N E126C, LF_N R263C and poly-lysine peptide (KKKKKAGNAGANAGAGC) beads were prepared as follows. Activated thiol sepharose beads (~2.5 g) were washed with 100 mL of water to remove all preservatives. Next, approximately 10 mL of 40 μM of both the LF_N constructs and peptide were prepared in 20 mM Tris-HCl buffer, pH 8.0, 150 mM sodium chloride and were mixed with the beads in a small conical tube. The suspension was incubated with agitation for 2 h at 4°C to insure adequate covalent attachment of the LF_N constructs and multi-lysine peptide onto beads. Activated thiol sepharose beads release 2-thiopyridone upon LF_N binding. The reaction progression was monitored by taking small aliquots of supernatant from the mixture as a function of time to monitor the decrease in protein absorbance at 280 nm and concomitant increase in 2-thiopyridone absorbance at 343 nm. The coupling reaction was continued until the absorbance increase at 343 nm no longer changes. At this time, supernatant was separated from beads and discarded. Beads were resuspended in pH 8.0 buffer (above) containing 20% glycerol and stored at -80°C for further use.

Preferential binding of PA to affinity beads. To test if some or all of the now-immobilized LF_N constructs can bind to the PA prepore, 100 μ L of an initial concentration of PA prepore (1.25 μ M) was applied to the various affinity beads (E126C, R263C and N-terminal unstructured peptide alone where the volume of beads was \sim 50 μ L). These mixtures were incubated for 10 min at room temperature (25°C), and the supernatant (flow through) was checked using both western dot blot and SDS PAGE densitometric analysis to determine if there was a decrease in unbound protein concentration. By this rough analysis, the binding capacity towards PA prepore was estimated to be 77, 41, and 48% for LF_N E126C, LF_NR263C and poly lysine beads, respectively. The highest binding efficiency under most conditions tested was obtained using the LF_N E126C construct. The binding conditions of the PA prepore to the LF_N E126C beads was checked throughout a pH range of 6.5–9.0 and under various sodium chloride concentrations between 5 and 500 mM to determine the best conditions.

Preparation of LF_N-PA pore in nanodiscs. PA prepore was found to bind preferentially to LF_N E126C affinity beads. About 50 μ L of beads were transferred to a mini-spin column (Pierce centrifuge columns 0.8 mL, Thermo scientific, USA) and washed with 50 mM NaCl, 50 mM Tris-HCl, pH 7.5 (buffer A) to remove preservatives. To these washed beads, 100 μ L of 0.2 μ M PA prepore, and 100 μ L 2M urea was added to the spin column containing the immobilized LF_N E126C affinity beads. The final concentration of urea was 1 M. Previous EM experiments showed that simply exposing PA to 1M urea at room temperature was insufficient to promote the conversion of the PA prepore to pore. After a short incubation period where PA became bound to the covalently attached LF_N, this mixture was heated to 37°C for 5 min to convert the LF_N-bound PA-prepore to the LF_N-bound PA-pore⁵ resulting in a transition to the pore pointed away from the bead surface. After PA conversion was complete (previous incubation times \sim 5 min), LF_N beads-PA-urea sample were centrifuged on a tabletop microfuge for 30 s to remove the supernatant and washed twice with 500 μ L of buffer A. The initial MSP1D1, POPC, and sodium cholate mixture was combined and incubated for 10 min prior to its addition to the LF_N-bound PA-pore beads slurry. Specifically, the His-tagged version of the MSP1D1, palmitoylcholine (POPC), and Na cholate mixture (2.5 μ M MSP1D1, 162 μ M POPC in buffer A containing 25 mM sodium cholate) were added to the prepared LF_N E126C affinity bead-PA pore complex to yield final volume mixture (400 μ L) containing approximately 0.2 μ M immobilized PA-pore heptamer. The

mixture, including the beads, was dialyzed with Spectra/Por Membranes molecular weight cutoff: 12–14,000 (spectrum) in excess buffer A for 8–12 h in the presence of 400 mg of bio-beads to accelerate cholate removal and nanodisc formation. The LF_N beads were collected after dialysis, washed 25 times with 400 μ L of buffer B (50 mM NaCl, 50 mM Tris-HCl, pH 7.5, and 5 mM EDTA) to remove any empty nanodiscs. The LF_N-PA-nanodisc complex was covalently uncoupled from the bead matrix (disulfide reduction) by incubating the mixture with 50 mM DTT (50 μ L prepared from 1M DTT stock) to the spin column containing beads with the newly formed LF_N-PA-nanodisc complexes. This column was sealed and the column contents were incubated for 30 min at room temperature using a gentle rotary wheel to insure complete reduction. The supernatant now containing the newly assembled LF_N-PA-pore-nanodisc complexes were centrifuged to separate the beads from the complex. The LF_N-PA-nanodisc complexes were applied to another spin column containing 50 μ L of Ni-NTA resin, which was preliminarily hydrated and equilibrated with 500 mM NaCl, 50 mM Tris-HCl pH 7.5, 10 mM imidazole (Buffer C) in order to bind the newly formed LF_N-PA-nanodisc through its MSP1D1 affinity His-tag. During this final incubation purification, 10 mM imidazole and 500 mM NaCl was also included to prevent non specific binding of PA to Ni-NTA column (as revealed in Ref. ⁶). After 10-min incubation, sample sizes of 50 μ L Ni-NTA resin immobilized complexes were spun down, the flow-through was discarded. The beads were washed twice with buffer C and then washed twice with a 50 mM NaCl, 50 mM Tris-HCl pH 7.5, 10 mM imidazole solution insure against any contamination from free PA and/or PA aggregates. To elute the LF_N-PA pore-nanodisc complex, 50 μ L of 100 mM imidazole was added to the \sim 50 μ L slurry volume of Ni-NTA beads, the mixture was incubated for 10 min on ice and the eluted LF_N-PA-nanodisc complex was prepared for electron microscopic analysis.

Negatively stained EM specimen preparation and data collection. For EM grid preparations, a diluted mixture of the LF_N-PA-nanodisc, estimated to be approximately 0.2 μ M in LF_N-PA, was applied to carbon-coated Cu 300 mesh grids and stained with 1% methylamine tungstate as described previously.⁶ Images were recorded on film using a minimal-dose procedure at a magnification of 60,000 \times using a JEOL 1200EXII electron microscope at defocus values between 0.6 and 0.7 μ m. The micrographs were digitized using a Microtek ScanMaker i900 scanner at a pixel size of 5.4 \AA on the specimen. Four micrographs were analyzed, each containing 100–150 nanodiscs, of which 40–50% had one or two PA molecules inserted.

Cryo EM specimen preparation and data collection. Thin solid carbon films were deposited over the holes of Quantifoil grids for use in cryoEM specimens. A nitrocellulose film was applied to the grids, coated with a minimal layer of evaporated carbon, and treated over ethyl acetate to remove nitrocellulose. About 3–4 μ L drops of freshly-prepared LF_N -PA nanodisc solutions at full concentration were applied to the grids at room temperature, adsorbed for 1–2 min, blotted in a humidified changer and dropped into liquefied ethane. Images were recorded on film on a JEOL 1200EXII at 100 kV using minimal doses, or on a CCD detector using a Tecnai F20 electron microscope (FEI, Eindhoven) at 200 kV at a magnification of 60,000 \times with 0.6–0.5 μ m underfocus.

Image processing and 3D reconstruction. The procedures followed were essentially the same as those reported previously.⁶ Briefly, the astigmatism and other optical defaults were visually inspected by recording power spectra for each micrograph. Alternating Conditional Expectation (ACE) MATLAB toolbox²¹ was used to estimate the defocus for each micrograph. Single particles were corrected for phase inversion and performed reference free 2D class averages with EMAN,²² 3D reconstruction was performed with the SPIDER software suite.⁹ Three-dimensional reconstruction was performed using projection matching²³ to two models: previously-calculated 3D structure of PA⁶ which is filtered to 100 Å resolution and a simple cylinder (radius 40 Å and height 180 Å), yielding visually identical results. Reconstructions were performed iteratively until fewer than 5% of the particles changed alignment. Three-dimensional structures were displayed at 100% volume of the proteins using Chimera.²⁴ Fitting of the PA pore structure derived from crystal structure of heptameric PA prepore (PDB 1TZO) by NMFF analysis⁶ into the LF_N -PA EM structures was done manually with Chimera.

References

- Krantz BA, Melnyk RA, Zhang S, Juris SJ, Lacy DB, Wu Z, Finkelstein A, Collier RJ (2005) A phenylalanine clamp catalyzes protein translocation through the anthrax toxin pore. *Science* 309:777–781.
- Feld GK, Thoren KL, Kintzer AF, Sterling HJ, Tang II, Greenberg SG, Williams ER, Krantz BA (2010) Structural basis for the unfolding of anthrax lethal factor by protective antigen oligomers. *Nat Struct Mol Biol* 17:1383–1390.
- Krantz BA, Finkelstein A, Collier RJ (2006) Protein translocation through the anthrax toxin transmembrane pore is driven by a proton gradient. *J Mol Biol* 355:968–979.
- Dmochewitz L, Lillich M, Kaiser E, Jennings LD, Lang AE, Buchner J, Fischer G, Aktories K, Collier RJ, Barth H. (2010) Role of CypA and Hsp90 in membrane translocation mediated by anthrax protective antigen. *Cell Microbiol* 13:359–373.
- Katayama H, Janowiak BE, Brzozowski M, Jurczyk J, Falke S, Gogol EP, Collier RJ, Fisher MT (2008) GroEL as a molecular scaffold for structural analysis of the anthrax toxin pore. *Nat Struct Mol Biol* 15:754–760.
- Katayama H, Wang J, Tama F, Chollet L, Gogol EP, Collier RJ, Fisher MT (2010) Three-dimensional structure of the anthrax toxin pore inserted into lipid nanodiscs and lipid vesicles. *Proc Natl Acad Sci USA* 107:3453–3457.
- Jennings-Antipov LD, Song L, Collier RJ. (2011) Interactions of anthrax lethal factor with protective antigen defined by site-directed spin labeling. *Proc Natl Acad Sci USA* 108:1868–1873.
- Steven JL, Matthew LB, Dong-Hua C, Jiu-Li S, David TC, Wah C (2008) De Novo backbone trace of GroEL from single particle electron cryomicroscopy. *Structure* 16:441–448.
- Frank J, Radermacher M, Penczek P, Zhu J, Li Y, Ladjadj M, Leith A (1996) SPIDER and WEB: processing and visualization of images in 3D electron microscopy and related fields. *J Struct Biol* 116:190–199.
- Janowiak BE, Jennings-Antipov LD, Collier RJ (2010) Cys-Cys cross-linking shows contact between the N-terminus of lethal factor and Phe427 of the anthrax toxin pore. *Biochemistry* 50:3512–3516.
- Ye F, Hu G, Taylor D, Ratnikov B, Bobkov AA, McLean MA, Sligar SG, Taylor KA, Ginsberg MH (2010) Recreation of the terminal events in physiological integrin activation. *J Cell Biol* 188:157–173.
- Pandit A, Shirzad-Wasei N, Wlodarczyk LM, van Roon H, Boekema EJ, Dekker JP, de Grip WJ (2011) Assembly of the major light-harvesting complex II in lipid nanodiscs. *Biophys J* 101:2507–2515.
- Mark PJ, Denisov IG, Grinkova YV, Sligar SG, Kincaid JR (2011) Defining CYP3A4 structural responses to substrate binding. Raman spectroscopic studies of a nanodisc-incorporated mammalian cytochrome P450. *J Am Chem Soc* 133:1357–1366.
- Yan R, Mo X, Paredes AM, Dai K, Lanza F, Cruz MA, Li R (2011) Reconstitution of the platelet glycoprotein Ib-IX complex in phospholipid bilayer nanodiscs. *Biochemistry* 50:10598–10606.
- Raschle T, Hiller S, Yu TY, Rice AJ, Walz T, Wagner G (2009) Structural and functional characterization of the integral membrane protein VDAC-1 in lipid bilayer nanodiscs. *J Am Chem Soc* 131:17777–17779.
- Frauenfeld J, Gumbart J, Sluis EO, Funes S, Gartmann M, Beatrix B, Mielke T, Berninghausen O, Becker T, Schulten K, Beckmann R (2011) Cryo-EM structure of the ribosome-SecYE complex in the membrane environment. *Nat Struct Mol Biol* 18:614–621.
- Bayburt TH, Sligar SG (2010) Membrane protein assembly into nanodiscs. *FEBS Lett* 584:1721–1727.
- Vernier G, Wang J, Jennings LD, Sun J, Fischer A, Song L, Collier RJ (2009) Solubilization and characterization of the anthrax toxin pore in detergent micelles. *Protein Sci* 18:1882–1895.
- Miller CJ, Elliott JL, Collier RJ (1999) Anthrax protective antigen: prepore-to-pore conversion. *Biochemistry* 38:10432–10441.
- Wigelsworth DJ, Krantz BA, Christensen KA, Lacy DB, Juris SJ, Collier RJ (2004) Binding stoichiometry and kinetics of the interaction of a human anthrax

- toxin receptor, CMG2, with protective antigen. *J Biol Chem* 279:23349–23356.
21. Mallick SP, Carragher B, Potter CS, Kriegman DJ (2005) ACE: automated CTF estimation. *Ultramicroscopy* 104:8–29.
 22. Ludtke SJ, Baldwin PR, Chiu W (1999) EMAN: semi-automated software for high resolution single-particle reconstruction. *J Struct Biol* 128:82–97.
 23. Penczek P, Grassucci RA, Frank J (1994) The ribosome at improved resolution: new techniques for merging orientation refinement in 3D cryo-electron microscopy of biological particles. *Ultramicroscopy* 53:251–270.
 24. Huang CC, Couch GS, Pettersen EF, Ferrin TE (1996) Chimera: an extensible molecular modeling application constructed using standard components. *Biocomputing: Proceedings of the 1996 Pacific Symposium*. Singapore: World Scientific, p724.